Integrative Biology

Accepted Manuscript

ROYAL SOCIETY OF CHEMISTRY

www.rsc.org/ibiology

Integrative Biology

ARTICLE

Acetate ion enhance load and stability of doxorubicin onto PEGylated nanodiamond for selectively tumor intracellular controlled release and therapy

Lin Li,[a] Lu Tian,[b] Wenjing Zhao,[b] Yingqi Li*[b, a] and Binsheng Yang*[a]

Received 00th January 20xx,
Accepted 00th January 20xx

DOI: 10.1039/x0xx00000x

www.rsc.org/

A successful drug delivery device for cancer chemotherapy should ideally be able to load drugs highly, bring the drug preferentially into tumor cells and reduce distribution in the normal tissue to enhancing therapeutic efficacy. To this purpose, a novel protocol for DOX loaded PEGylated nanodiamond (ND-PEG-DOX/NaAc, NPDA) was fabricated using sodium acetate medium. The NPDA nanoparticles exhibited a maximum loading efficiency (99 wt%) with ultra-low drug leakage (7 wt%). Confocal microscope and flow cytometer showed that the NPDA uptake by cells was time-dependent and a slow and sustained drug release from the lysosomes with a low pH. Besides, CHO (a normal cell) and MCF-7 (a cancer cell) were treated with NPDA, respectively, the result indicated that NPDA preferentially accumulated much more in tumor cells rather than normal cells, which demonstrate the ability of NPDA to selectively kill tumor cells. In addition, NPDA can inhibit the migration and proliferation of tumor cells and change the cell cycle compared to free drug. Outcomes from this work suggest that NPDA would be a promising drug delivery platform and the preparation of such a drug delivery system will also have implications in improving the biomedical applications of the smart nanodiamonds carriers.

Insight, innovation, integration

Nanodiamond as a carrier for transporting chemotherapy drugs has emerged as a promising strategy for treating cancer. However, several factors limited its extensive applications in biology, such as low drug loading, easily cluster and a high drug loss under physiological environment. In this work, to ensure high drug capacity and low drug leakage in physiological conditions, and especially ensure to be delivered to tumor region, a selectively tumor intracellular controlled release drug delivery system was designed and prepared by DOX adsorbed onto PEGylated nanodiamond in sodium acetate medium (ND-PEG-DOX/NaAc, NPDA).This study introduces a simple and effective strategy to design a promising drug delivery platform for improving the biomedical applications of the smart nanodiamonds carriers.

Introduction

From time immemorial, cancer, a disease that is difficult to be diagnosed earlier and treated thoroughly, has always been an invincible opponent to human beings.[1-3] Among the therapeutic regimens of cancer, conventional chemotherapy, which conveys anticancer drugs systemically to patients sequentially to kill cancerous cells, is the prevailing-most frequent treatment.[4,5] However, anticancer drugs, which possess some drawbacks, such as metabolic trapping, multidrug resistance, nonspecific targeting and severe toxicities including serious organ damage, have been greatly restricted.[6,7]

Nanotechnology, an interdisciplinary research encompassing chemistry, biology, engineering and medicine, brings the gospel to cancerous person that can approaches the weakness of anticancer drugs in cancer treatment.[8-10] Nanoparticles, which exert good superiorities, such as, small size effect,[11] larger surface area,[12] unusual physical properties[13] and modifiable surface properties,[14] occupy a unique position in the cancer therapy.[15] Since 1950, different kinds of nanoparticles were applied to drug delivery, for instance, liposomes,[16] polymer,[17] polymer-lipid hybrid,[18] dendrimers,[19] hydrogels,[20] phase-change materials[21] and inorganic nanoparticles.[22, 23]

Among the inorganic nanoparticles, carbon nanotubes,[24] graphene oxide,[25] fullerene,[26] mesoporous silicons[27] and nanodiamond[28] are widely researched in cancer therapy due to their high surface area and pore volume, excellent physicochemical properties, easily functionalizable surfaces, good biocompatibility and little immunogenicity.

Nanodiamonds (NDs), which are equipped with the best biocompatibility, good optical property,[29] stable fluorescence

[a] Key Laboratory of Chemical Biology and Molecular Engineering of Ministry of Education, Institute of Molecular Science, Shanxi University, Taiyuan 030006, PR China. *E-mail:, yangbs@sxu.edu.cn
[b] Department of Chemistry, College of Chemistry and Chemical Engineering, Shanxi University, Taiyuan 030006, PR China. *E-mail: wkyqli@sxu.edu.cn

Electronic Supplementary Information (ESI) available: [Stability, cell viability with time, cell morphology and cellular uptake kinetics]. See DOI: 10.1039/x0xx00000x

Integrative Biology

without photobleaching or photoblinking[30] and modifiable surface property,[31] allow for improvement of numerous cancers therapy. Unfortunately, the easily agglomeration of NDs have somewhat limitation to achieve a scope biology application.[32] To overcome the obstacle, such as protein[33] and PEG[34] et al are introduced to improve the dispersibility. PEG, a hydrophilic macromolecular that is conducive to prolong the circulation time by minimizing opsonization, reduce phagocytosis and complement activation, has been widely adopted to modify all kinds of nanoparticles.[35,36] For example, Zhang *etal* developed surface modification of CNT with poly PEGMA via combination of mussel inspired chemistry and chain transfer free radical polymerization for the first time.[37] We prepared ND–PEG via an ester band and found that PEGylated ND showed enhanced dispersity and stability in vitro under physiological conditions or in cell culture medium in our previous study.[38] Xu *etal* proposed nanoscale drug delivery system based on PEGylated graphene oxide (GO) to improve the utilization rate of paclitaxel (PTX).[39] We also employed PEGylated NDs to deliver DOX, an apoptosis-inducing chemotherapy drug that is widely used to treat many kinds of cancers, and demonstrated that it could improve treatment efficiency and decrease toxicity to normal tissues.[40] However, a fly in the ointment is the drug loading onto ND only to achieve 3 % - 5 %. Improvement of DOX adsorption to PEGylated NDs may prove vital in enhancing DOX effectively treatment in cancer and decreasing side effects.

In this study, we present a novel technique for DOX adsorbing onto PEGylated NDs yielding higher loadings than previously reported ND-PEG/DOX systems.[38] Specifically, carboxylated ND was conjugated by polyethylene glycol amine carboxyl (H_2N-PEG-COOH) to obtain the ND-PEG-COOH nanocarrier. In the following step, DOX was successfully coated onto the ND-PEG-COOH in the sodium acetate medium via hydrogen bonds and van der Waals´ forces, to obtain ND-PEG-DOX/NaAc (NPDA) nanoparticles. We found that the addition of NaAc is an essential component of the loading process and the salt was shown to be able to promote the adsorption of DOX onto the PEGylated NDs, where nearly 99 wt% adsorption of DOX on the ND-PEG-COOH was achieved in the sodium acetate medium (NaAc, 1.0M). The NPDA was found to move inside the cells quickly and was capable of delivering the drug inside living cells efficiently. In addition, MTT assays were applied to evaluate the therapeutic efficacy of NPDA. Besides, CHO (a normal cell) and MCF-7 (a cancer cell) were treated with NPDA, respectively, the result indicated that NPDA preferentially accumulated in tumor cells rather than normal cells, which demonstrate the ability of NPDA to selectively kill tumor cells. As such, this work convincingly demonstrates the potential of ND as a broad drug-delivery platform, which could potentially decrease drug toxicity to normal cells/tissue.

Materials and methods

Materials and instruments

Synthetic type 1b nanodiamond powders (ND) commercially available (sizes ≈140 nm, Element Six) were chosen here because the tumor blood vessels can retain 100-400 nm particles. Then the nanodiamond powders were carboxylated[40] to use throughout the experiment. Doxorubicin hydrochloride (DOX) was purchased from Shanxi pude Pharmaceutical Co., Ltd. (China). Polyethylene glycol amine carboxyl (H_2N-PEG-COOH) was bought from Shanghai seebio Biotech Inc, China. Lyso-Tracker Red, N-hydroxy succinimide (NHS), 2-(N-morphine) ethane sulfonic acid (MES) and 1-(3-dimethylaminopropyl)-3-ethyl carbodiimide hydrochloride (EDC) were purchased from Sigma. (M-β-CD) were purchased from Shanghai Aladdin Reagent Co., Ltd. (China). 3-(4, 5-dimethylthiazol-2-yl)-2, 5-diphenyltetrazolium bromide (MTT), Green streptomycin mixture and paraformaldehyde were purchased from Solarbio (Beijing, China). Dulbecco Minimum Essential Media (DMEM) was purchased from Thermo Fisher Biological and Chemical Product (Beijing, China). Fetal bovine serum was purchased from Hangzhou Sijiqing Biological Engineering Materials Co., Ltd (China). Trypsin was purchased from Sino-American Biotechnology Company. Hoechst 33258 was purchased from Beyotime Biotechnology (in China). Sucrose was purchased from Amresco Co. (USA). HeLa, HepG2, MCF-7 and CHO cells were provided by the Gene Engineering Center of Shanxi University. All other chemicals and solvents were of analytical grade and procured from local suppliers unless otherwise mentioned. Millipore filtered water was used for all aqueous solutions.

Fluorescence spectrophotometer (970CRT, Shanghai Analytical Instruments Factory), UV-vis spectrophotometer (UV1901, Beijing spectral analysis of GM), Ultrasonic cleaner (KQ-100DE, Kunshan Ultrasonic Instrument Co., L,), High speed micro-centrifuges (TG16-W, Hunan Instrument Laboratory Instrument Development Co., Ltd.), Flip shake instrument (DR-MIX, Beijing Hao North Biotechnology Co., Ltd.), Air oscillator (THZ-22, Taicang City Experimental Equipment Factory), Fourier transform infrared spectroscopy (FTIR-8400S, Shimadzu Corporation, Kyoto, Japan), Malvern Nano Particle Sizer (ZETA Sizer, Nano-ZS90, England), Autoclave (YX280B, Shanghai Medical Devices Co., Ltd.), Transmission electron microscopy (JEM-2100, JEOL, Japan), Vacuum drying oven (DZF-6020, Shanghai Yiheng Scientific Instrument Co., Ltd.), Thermostat water bath (ZDKW-4, Beijing Zhongxing Weiye Instrument Co., Ltd.), Inverted microscope (MI11, Guangzhou Mingmei Technology Co., Ltd.), Optical microscope (XSP-8CA, Shanghai Optical Instrument Factory), Clean bench (YT-CG-1ND, Beijing Both Cologne Experiment Technology Co., Ltd.), Full automatic microplate reader (Model 550, Bio-Rad, USA), Flow cytometer (FACS Calibur, BD, USA), Laser scanning confocal microscope (Leica TCSSP5, Germany).

Optimization and preparation of ND-PEG-DOX/NaAc

The concentration effect of sodium acetate medium on DOX adsorption. First, ND-PEG was prepared according to previously reported method by us.[40] Then five 1 mg of ND-PEG nanoparticles were sonicated at 100 W for 1 h in 1 mL of different concentration of sodium acetate medium (0.05 M, 0.1 M, 0.2 M, 0.6 M and 1.0 M). Next, 200 μg of doxorubicin was added, and the suspension was shaken and protected from light at room temperature for 6 h. Finally, the suspension was centrifuged at 15000 rpm for 5 min, and the precipitate was washed three times with deionized water to remove the unadsorbed DOX. The amount of DOX adsorbed was determined by calculating the change in DOX concentration before

and after adsorption using an ultraviolet-visible spectrophotometer at 500 nm.

Time effect on DOX adsorption. Based on the optimum concentration effect between ND-PEG and DOX, the optimum reaction time between ND-PEG and DOX was also investigated in sodium acetate medium (1.0 M) using the technique as previously reported by us.[40]

Drug loading efficiency. Based on the optimum concentration effect and reaction time between ND-PEG and DOX, the amount of drug loading was further researched, where the concentrations of DOX were 100, 200, 500, 600, 1000 μg·mL^{-1} and the concentration of ND-PEG was 1 mg·mL^{-1} for all solutions in sodium acetate medium (1.0 M) for 6 h. Then the solutions were centrifuged at 15000 rpm for 5 min to remove excessive DOX. As previous reported,[41] briefly, the supernatants were removed, and their absorbance was read from 200 to 800 nm at ambient temperature with a UV-visible spectroscopy. The peak absorbance of DOX was found at 500nm. The difference in added DOX and DOX in the supernatant yielded the amount of DOX adsorbed. The drug loading efficiency and drug loading percentage on ND-PEG were assessed using the following equations (1) and (2), respectively:

$$\frac{\text{DOX (μg)}_{\text{Adsorbed}}}{\text{DOX (μg)}_{\text{Added}}} \times 100\% \quad (1) \qquad \frac{\text{DOX (μg)}_{\text{Adsorbed}}}{\text{ND-PEG (μg)}_{\text{Added}}} \times 100\% \quad (2)$$

Preparation of ND-PEG-DOX/NaAc. In the subsequent experiments, the NPDA nanoparticles with DOX loading of 195.0 μg·mg^{-1} was characterized and studied. ND-PEG (1 mg) was dispersed in the sodium acetate medium (1.0 M) and sonicated for 1 h, DOX (200 μg) was then added and the mixture was shaken up at room temperature for 6 h. NPDA thus obtained by centrifugation at 15000 rpm, rinsed with deionized water for three times and then placed in a vacuum drying oven and protected from light. The amount of absorbed DOX was measured by calculating the difference value of the total DOX and the supernatant DOX.

Characterization of ND-PEG-DOX/NaAc

Fourier transform infrared spectroscopy (FTIR) and UV-visible spectroscopy were used to confirm the presence of DOX and PEG on the surface of ND. Transmission electron microscopy (TEM) was used to visually confirm the coupling of ND with PEG and DOX. A Zeta-sizer Nano ZS90 was used to monitor the zeta potential, polydispersity index (PDI) and hydrodynamic size of the ND before and after modification. Measurements of nanoparticles size were performed at 25 °C and a scattering angle of 90°. The mean hydrodynamic diameter was determined by cumulative analysis. Determination of the zeta potential was based on electrophoretic mobility of the nanoparticles in aqueous medium, and was performed using folded capillary cells in automatic mode.

pH-Dependent release of DOX from NPDA

The release of DOX from NPDA in different pH was evaluated by a dialysis method. First, the same amount of complex was suspended in PBS of pH 7.4, pH 6.5, pH 5.0 and ABS of pH 4.5 with sonication at room temperature for 30 min, respectively. Next, the suspensions were placed into dialysis bags and subsequently placed into a 50 mL centrifuge tube containing the buffer solutions, respectively. The centrifuge tubes were then placed in the air oscillator maintained at 37 °C at 150 rpm. The volume of the buffer solutions in the tubes was maintained at 9 mL. At predetermined time intervals, the buffer solutions was removed and replaced with fresh medium. Dialysates were analyzed by UV-vis spectrophotometry to determine the concentration of dissociated DOX from NPDA and the cumulative release rate. The experiment was performed in triplicate. The data were averaged, and standard deviations were calculated.

Cell culture

Human hepatoma cells (HepG2 cells), Human cervical cancer cells (HeLa cells), Human breast cancer cells (MCF-7 cells) and Chinese hamster ovary cells (CHO cells) were cultured in a 10 cm Petri dish with a glucose Dulbecco's modified Eagle's minimal essential medium (DMEM) containing 10 % fetal bovine serum (FBS) and 1 % penicillin-streptomycin at 37 °C and 5 % CO_2 in a humidified incubator, respectively. Cells were subcultured regularly using trypsin/EDTA.

In vitro cytotoxicity

To examine the anti-tumor effect of NPDA nanoparticles, free DOX and ND-PEG acted as controls in the experiment. The cytotoxic potential of the NPDA was assessed with an MTT assay. HepG2, HeLa and MCF-7 cells (5×10^3 cells/well) were seeded in 96-well culture plates and allowed to adhere for 16 h, respectively. Then the cells were treated with ND-PEG, NPDA (5 μg·mL^{-1} of DOX equivalent) or free DOX (5 μg·mL^{-1}) for 24 h, 48 h and 72 h, respectively. After that, treated cells were further incubated with 20 μL of MTT (5 mg·mL^{-1}) each well for additional 4 h. The medium was then removed, and 150 μL of DMSO was added into each well for dissolution of the formazan crystals formed by living cells. After 10 min's shaking, absorbance at 490 nm was measured using a Microplate reader. Cell viability was expressed as a percentage of the absorbance to that of the control experiment without treatment. The data recorded represented the means of sixplicate measurements.

In vitro wound scratch assay

The effect on cell migration inhibition of NPDA was evaluated by in vitro scratch assay. MCF-7 cells were seeded into each well of 6 well tissue culture plates to a final density of 2×10^5 cells per well and these were maintained at 37 °C and 5 % CO_2 for 24 h until the cell adhered completely and the confluent monolayer formed. Therewith, using a sterile micro pipette tip to fabricate a scratch wound across each well, and the cell debris was removed and the edge of the scratch was smoothed by washing with PBS (pH 7.4). Subsequently, the fresh medium with ND-PEG, NPDA and free DOX were added into corresponding well and incubated unceasingly. The cells without treatment were used as the control. The change of wound healing was monitored by collecting micrographs at various time intervals with an inverted microscope and the width of the scratch was measured with the imaging software system. Each well

Integrative Biology

was marked below the plate surface by drawing a vertical line, to allow identification of the same scratched area in order to take consistent pictures. Scratch area was measured using Image J software. Migration rate was expressed as percentage of scratch closure on an initial area basis, according to the following equation:

$$\mathrm{WC} = \left(1 - \frac{\mathrm{SW_t}}{\mathrm{SW_0}}\right) \times 100\%, \quad \mathrm{MIR} = \left(1 - \frac{\mathrm{WC_{treatment}}}{\mathrm{WC_{control}}}\right) \times 100\%$$

where SW_0 and SW_t stand for the scratch width of 0 h and given time, respectively, $WC_{treatment}$ and $WC_{control}$ stand for the wound closure rate of treatment and control groups.

Cellular uptake

The cellular uptake of NPDA was visualized via a laser confocal scanning microscopy to acquire the fluorescence images of the internalized NPDA nanoparticles in MCF-7 cells, which as a representative of investigating NPDA uptaken by cells. Briefly, MCF-7 cells at a density of 1.0×10^3 cells per dish were plated onto glass-bottomed 35 mm plates in 1 mL of complete culture medium for 16 h before treatment. Next the cells were treated with the nanoparticle in culture medium (5 μg·mL^{-1} of DOX equivalent) for 2 h, 5 h and 21 h, respectively. Then the medium was removed and washed thrice with ice-cold PBS. The cells were finally fixed with a 4 % paraformaldehyde solution for 8 min and stained with Hoechst 33258 (10 μg·mL^{-1}) for 15 min to label the nucleus. The stained cells were imaged under a laser scanning confocal microscope. Samples stained with H33258 and DOX were visualized with excitation wavelengths of 405 nm and 488 nm, respectively.

To further determine the position of the NPDA nanoparticle in cells, the red lyso-tracker probe was introduced. Briefly, MCF-7 cells were incubated with NPDA (3 μg·mL^{-1} of DOX equivalent) in DMEM with 10 % FBS for 5 h. At this time, free NPDA were removed by washing the cells 3 times with PBS. Then red lyso-tracker probe was added to continue incubation for 5 min. After that, red lyso-tracker probe was removed by washing the cells 3 times with PBS. Cells were then fixed with 4 % paraformaldehyde (300 μL) for 8 min at room temperature. The fluorescence of DOX was collected from 530 to 580 nm, and the fluorescence of lyso-tracker probe was collected from 655 to 755 nm (excitation wavelengths of 568 nm).

Besides, to study the tumor selective ability, Chinese hamster ovarian cell (CHO) was used as a model of normal cell and treated with NPDA (5 μg·mL^{-1} of DOX equivalent) for 5 h. Then cells were finally fixed with a 4 % paraformaldehyde solution for 8 min and stained with Hoechst 33258 (10 μg·mL^{-1}) for 15 min to label the nucleus. The stained cells were imaged under a laser scanning confocal microscope. Samples stained with H33258 and DOX were visualized with excitation wavelengths of 405 nm and 488 nm, respectively.

Cell apoptosis and cell cycle

Quantitative assessment of apoptosis was analyzed by an annexin V-FITC assay kit. In brief, MCF-7 cells were plated in 35 mm Petri dishes at a density of 1×10^5 and incubated at 37 °C with complete medium for 16-20 h. After that, the worn-out culture medium was replaced with fresh medium containing NPDA at 5 μg·mL^{-1} of DOX equivalent and incubated for another 48 h. Then the cells were harvested with trypsin and washed in PBS. Afterwards, cells were then resuspended in a binding buffer and stained with annexin V-FITC and PI at room temperature for 15 min kept from light. Finally, the stained cells were analyzed using FACS Calibur and Cell Quest software.

The cell cycle phases can be separated into G0/G1, S and G2/M by flow cytometer analysis. To examine the effect of NPDA on the cell cycle progression, MCF-7 cells were plated at a density of 1×10^6 cells per 60 mm Petri dish in complete medium for 16-20 h. After treatment for 30 h with nanoparticles, the cells were collected and fixed with ice-cold 70 % ethanol overnight at 4 °C. Thereafter, the cell pellets were treated with Propidium iodide (PI) solution containing RNase for 30 min at room temperature in the dark. Finally, the samples were analyzed by a Flow cytometer. At least 10 000 cells were analyzed for DNA content.

Results and discussion

Preparation and characterization of ND-PEG-DOX/NaAc

As shown in Fig. 1, to prepare modified ND, an amidation reaction was performed to create an amide bond between the carbonyl group of ND and the amine group of H_2N-PEG-COOH. Then the DOX was physically absorbed onto ND-PEG nanocarriers via hydrogen bonds and van der Waals´ forces, with the help of 1.0 M NaAc (pH 9.87), which is an essential component. The amount of generated carboxylic acid group on the inert nanodiamond surface following the oxidation process was measured using a potentiometric conductometric anti-titration method and concentrations of 114±0.8 μmol carboxylic acid per g of oxydic ND were calculated in three repeated experiments.[42,43]

To improve the amount of drug loaded onto the ND-PEG nanoparticles, first, the adsorption of DOX in different concentrati-

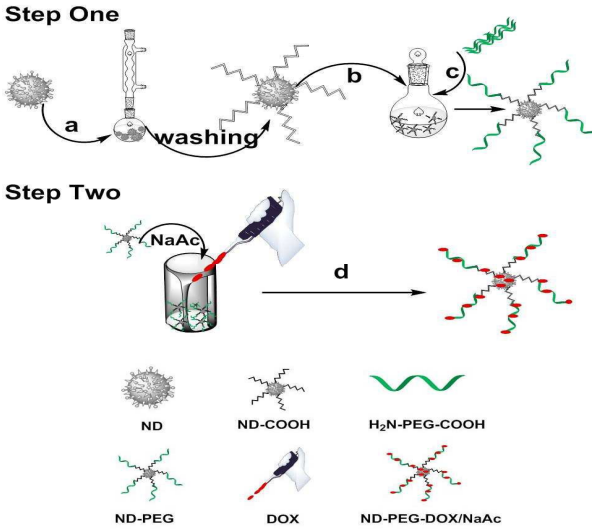

Fig. 1 Schematic of adsorption protocol for preparing ND-PEG-DOX/NaAc nanoparticles. The succession of synthetic processes is the following: (a) HNO_3:H_2SO_4 = 1:3, 90 °C, 3 d; 1 M NaOH, 90 °C, 2 h; 1 M HCl, 90 °C, 2 h; (b) EDC, NHS, rt, 6 h; (c) H_2N-PEG-COOH, BBS (pH 8.4), overnight; (d) DOX, NaAc (1.0 M), rt, 6 h.

on of NaAc was explored to obtain the absorption curve, as shown in Fig. 2A. We can observe that the amount of DOX loaded increased with increasing concentration of NaAc and finally reached saturation as the concentration increased to 1.0 M. As displayed in Fig. 2B (inset), compared with the original DOX solution (right photo), the suspension of ND-PEG-DOX/ NaAc (NPDA) nanoparticles showed pale red color (left photo). Besides, the amount of DOX as a function versus time was displayed in Fig. 2B. One can observe that

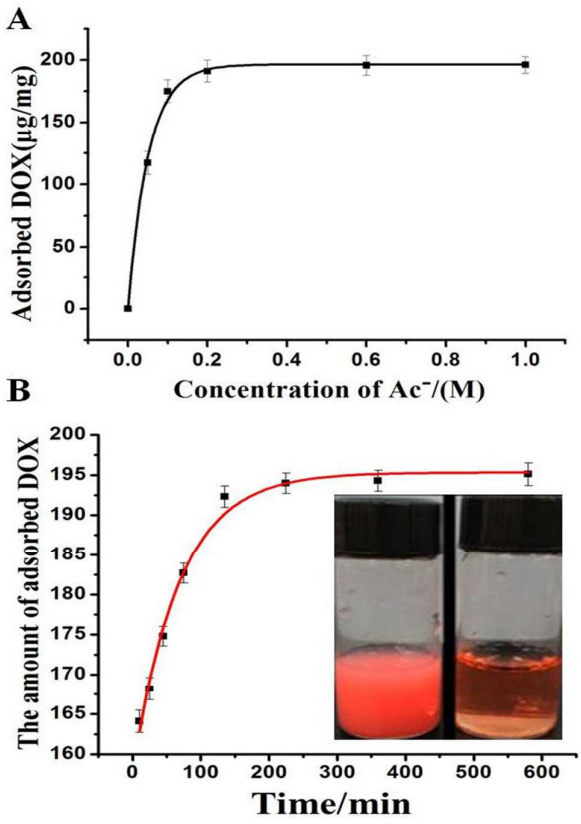

Fig. 2 Optimal conditions for preparing the NPDA system. (A) Determination of the best concentration of NaAc for adsorption of DOX. (B) Determination of the best time for adsorption of DOX.

Table 1 Summary of added DOX, adsorbed DOX, DOX loading efficiency and DOX loaded on ND-PEG.

DOX added (μg)	DOX adsorbed (μg)	DOX loading efficiency (wt %)	DOX loaded on ND-PEG (wt %)
100	95.9±0.2	95.0±0.2	9.6±0.1
200	195.0±1.9	97.5±0.9	19.5±0.1
500	497.0±1.3	99.4±0.5	49.7±0.3
600	595.0±1.1	99.2±0.3	59.5±0.3
1000	992.0±2.0	99.2±1.0	99.2±0.3

the adsorption of DOX by ND-PEG nanoparticles in the sodium acetate solution quickly reached equilibrium after 6 h incubation, which follows the first-order kinetics and the rate constants was calculated as 0.88 h^{-1}. In the system, the amount of DOX adsorbed was determined through converting the UV–vis absorbance to concentration using linear regression equation (Fig. S1).

Table 1 summarizes the adsorbed DOX, DOX loading efficiency, and DOX loading on ND-PEG. NDs adsorbed 195 μg of the added 200 μg DOX, which yielded a 97.5 % loading efficiency. A 99.4 % loading efficiency was achieved when 497 μg of the added 500 μg DOX was adsorbed. When 1000 μg DOX was added, the ND-PEG adsorbed approximately 992 μg DOX corresponding to a DOX loading efficiency of about 99.2 %. Since 1.0 mg of ND-PEG nanoparticles were used, loadings of DOX on the ND-PEG can up to 99.2 % for the added 1000 μg DOX. Up to now, the DOX loading onto ND or ND-PEG with the adsorption technique was the highest efficiency. We present almost a hundred percent in DOX loading on the ND-PEG to obtain the optimal ND-PEG/DOX, where sodium acetate is crucial to promote adsorption. From this point of view, sometimes a small anion plays a very important role (Fig. S2).

Besides, NPDA nanoparticles illustrated rather high stability (Fig. S3), where the NPDA nanoparticles were allowed to be stood at 4 °C and PBS medium (pH 7.4) for about 450 days to find the leakage rate of less than 7 %.

NPDA was successfully synthesized using a novel adsorption technique developed with sodium acetate medium (1.0 M). To confirm synthesis, the surface chemistry, morphology, particle size and zeta potential of NPDA were characterized. Formation of a functional group in ND preparations was characterized by FTIR spectroscopy in each step to confirm if the carboxyl and amide groups had been successfully attached onto the surface of ND during oxidation and amidation reactions respectively. Fig. 3A clearly indicates a gradual change in the creation of functional groups of carboxylic acid and the formation of the amidic linkage between ND and H_2N-PEG-COOH. As expected from the structure of oxydic ND, the absorbance at 3422 cm^{-1} and 1747 cm^{-1} is related to the hydroxyl group and carbonyl group of carboxylic acid. The absorbance band at 1656 cm^{-1} and 1621 cm^{-1} correspond to the C=O stretching and N-H bending of amide bonds of PEG grafted to ND. The spectra of NPDA showed absorbance at 1640 cm^{-1} and 1413 cm^{-1} are assigned to O-H stretching of carboxyl in NaAc and the phenyl ring vibration of DOX moiety, which are in consistent with the characteristic FTIR spectrum of NaAc and DOX as black arrow indicated.

The successful adsorption of DOX onto ND-PEG was also confirmed by UV-vis absorption. The UV-vis absorption spectrum of DOX, ND, ND-PEG and NPDA are shown in Fig. 3B. NPDA displayed the same absorption band like free DOX at 480 nm, demonstrating that DOX moiety is absorbed on ND-PEG.

Transmission electron microscopy (TEM) was used to further verify the formation of the intermediates and NPDA complex. Fig. 3C shows the typical images before and after coating with different molecules. Clear structures were visible in samples of ND and ND-PEG-COOH, the structures of ND were markedly less visible after the formation of NPDA. It can be obviously seen that NPDA was different from the first two materials, where single ND particle was

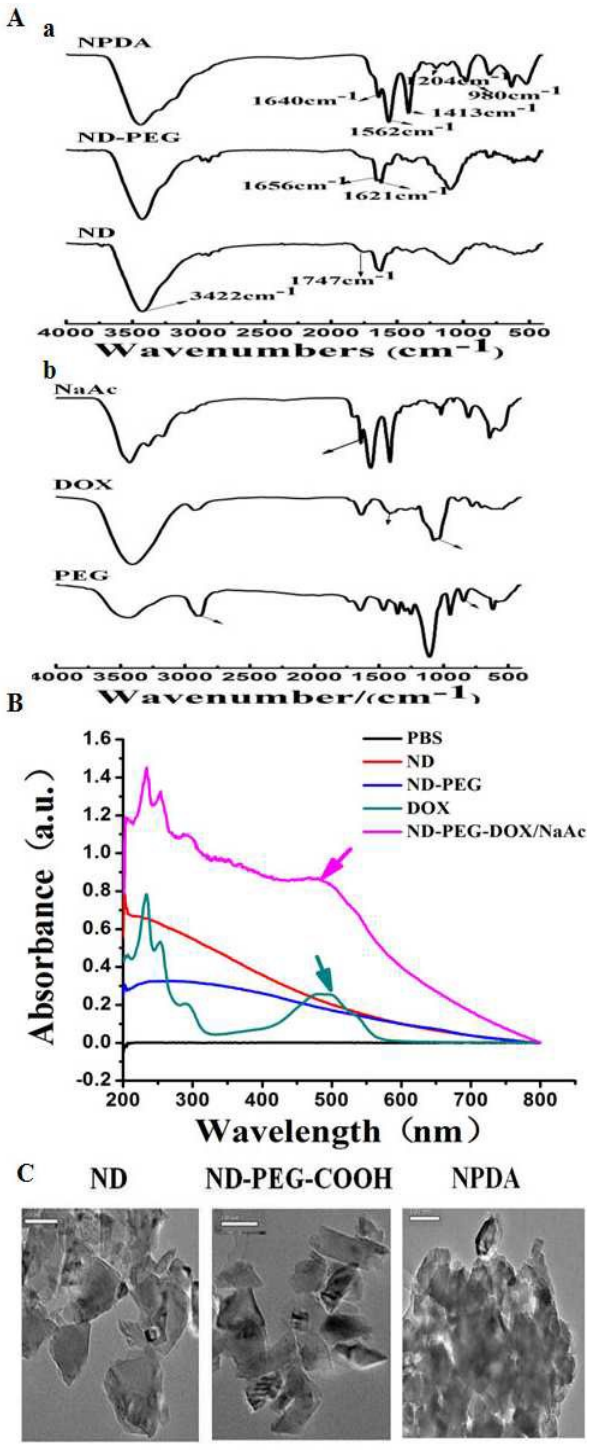

Fig. 3 Characterization of NPDA. (A) FTIR Spectra of various materials, (a) ND, ND-PEG and NPDA, (b) PEG, DOX and NaAc, where the arrows indicated the characteristic absorption peaks of corresponding functional groups; (B) UV-vis absorption of DOX, ND, ND-PEG and NPDA in PBS, where the arrows indicated the absorption peaks of DOX and NPDA. (C) Typical transmission electron microscopic images before and after coating with different molecules, respectively. The scale bars represent 100nm.

Table 2 Particle size, Zeta potential and PDI of ND, ND-PEG and NPDA

	Diameter (nm)	Zeta potential (mv)	PDI
ND	166.0±1.6	-30.2±1.0	0.164
ND-PEG	184.6±6.4	-24.7±1.9	0.126
NPDA	242.0±5.0	-23.7±0.8	0.108

hardly found and dark and thicker area formed, implying that the DOX coated on the surface of ND-PEG.

Based on DLS results (Table 2), the size of pristine ND is about 166 nm, which increased to 184.6 nm after grafted to PEG and more increased to 242.0 nm after loading with DOX. The increase in nanoparticle size after PEGylation could be attributed to the stretch of PEG chains on the PEGylated ND surface and the larger size of NPDA demonstrated the successful preparation. Besides, the polydispersity index (PDI) of ND (0.164), ND-PEG (0.126) and NPDA (0.108) also measured, as shown in Table 2, with the PEG grafting and DOX loading, the PDI gradually decreased, which indicated that the dispersity of nanoaprticles was improved accordingly. Measurement of zeta potential is used to discuss the density of acidic sites on the surface of ND. As expected, PEGylated ND (-24.7 mV) has less charge than oxydic ND (-30.2 mV) because of the conversion of carboxylic acid groups into amide groups during the PEGylation process. There was a little increase in zeta potential observed for NPDA (-23.7 mV) indicating successful coupling of DOX with ND-PEG. A similar observation has been confirmed by our previous report.[38,40]

The effect of pH on DOX release from ND-PEG-DOX/NaAc

For the successful application of ND as a drug delivery platform, it is important that specific and sustained drug release occur only upon reaching the target site. Premature release of DOX will induce toxicity in the blood circulatory system, such as damage to normal cells, tissues or metabolic breakdown. Since the nanoparticles may interact with cells in the body, where the pH ranges from 7.4 to 4.5, drug release from nanoparticles by environment pH stimuli is prerequisite to result in minimizing toxicity toward normal tissue. The in vitro release behavior of NPDA was evaluated under a simulated physiological condition (pH 7.4) and in the acidic environment (pH 4.5, pH 5.0 and pH 6.5) at 37 °C. The release profiles of DOX from NPDA at different pH values are presented in Fig. 4. The result revealed that the drug release rate was significantly dependent on the pH. In pH 7.4, the NPDA exhibit high stability with less than 10 % DOX release over a period of 70 h, while showed a fast release in the acidic environment and with the decrease of pH, the release amount of DOX was gradually increasing, at pH 6.5 (a simulated tumor environment) and pH 5.0 (a simulated endosomes environment), NPDA released about 20 % and 35 %, respectively. When the pH was decreased to 4.5 (simulated lysosome environment), the released DOX was increased nearly 60 %, which is six folds to the release of physiological condition, as it was expected that the NPDA nanoparticles had

minimal drug release (under simulated physiological conditions, pH7.4), but much

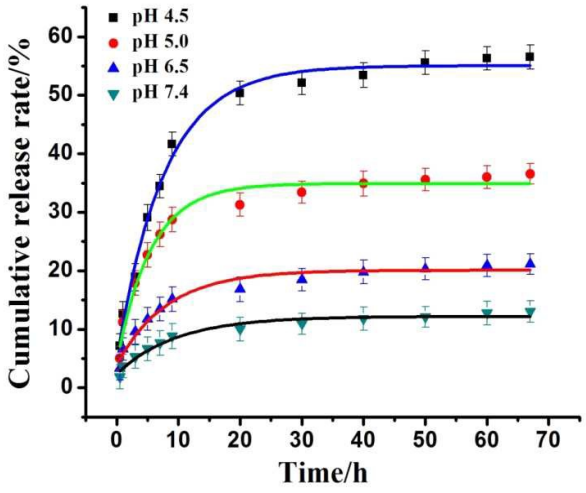

Fig. 4 The pH-responsive drug release profiles of DOX from NPDA at pH 7.4, 6.5, 5.0 and 4.5.

more DOX were released in acidic lysosome of cells (pH 4.5-5.0). The pH-triggered drug release behaviour of the NPDA was predominantly associated with the hydrogen bonds damage between amino of DOX and carboxy of Ac^-. According to the previous work,[44] the release of unmodified DOX achieved 54 % at pH 7.4; in comparison with NPDA, free DOX can damage cells in a normal physiological environment, causing serious side effects. The results suggested the NPDA drug delivery system has potential applications for controlled and sustained drug release.

Cytotoxicity assay

Considering the high drug-loading efficiency and excellent stability, NPDA nanoparticles might be a promising drug delivery system for cancer therapy. Thus, the in vitro cytotoxicity of the NPDA was evaluated at an equivalent dose of DOX (5 $\mu g \cdot mL^{-1}$) for different time periods. Typically, the tumor cells (HepG2, HeLa and MCF-7 cells) were first cultured overnight for adherence and then incubated with ND-PEG, NPDA and free DOX for 24 h, 48 h and 72 h, respectively. Fig. 5 shows that both NPDA and free DOX inhibit the proliferation of cancer cells in a time-dependent fashion. After 24 h incubation, NPDA exhibit low abilities of proliferation inhibition in cancer cells, while free DOX show an apparent inhibition. With the increase of incubation time to 72 h, the NPDA display markedly improved abilities of proliferation inhibition in the cancer cells that similar to the free DOX, which indicate that NPDA has slow release behaviour as demonstrated in vitro drug release. Moreover, there was no noticeable difference in cell viability between the ND-PEG groups and the control groups, which showed that the ND-PEG has a good biocompatibility.

HepG2, HeLa and MCF-7 cells were further incubated with various concentrations of ND-PEG, NPDA and free DOX, and their relative cell viabilities are shown in Fig. S4. It can be seen that ND-PEG displayed very little toxic effects on HepG2, HeLa and MCF-7 cells, with survival rates of more than 90 %. Both free DOX and NPDA were found to inhibit HepG2, HeLa and MCF-7cells, and the

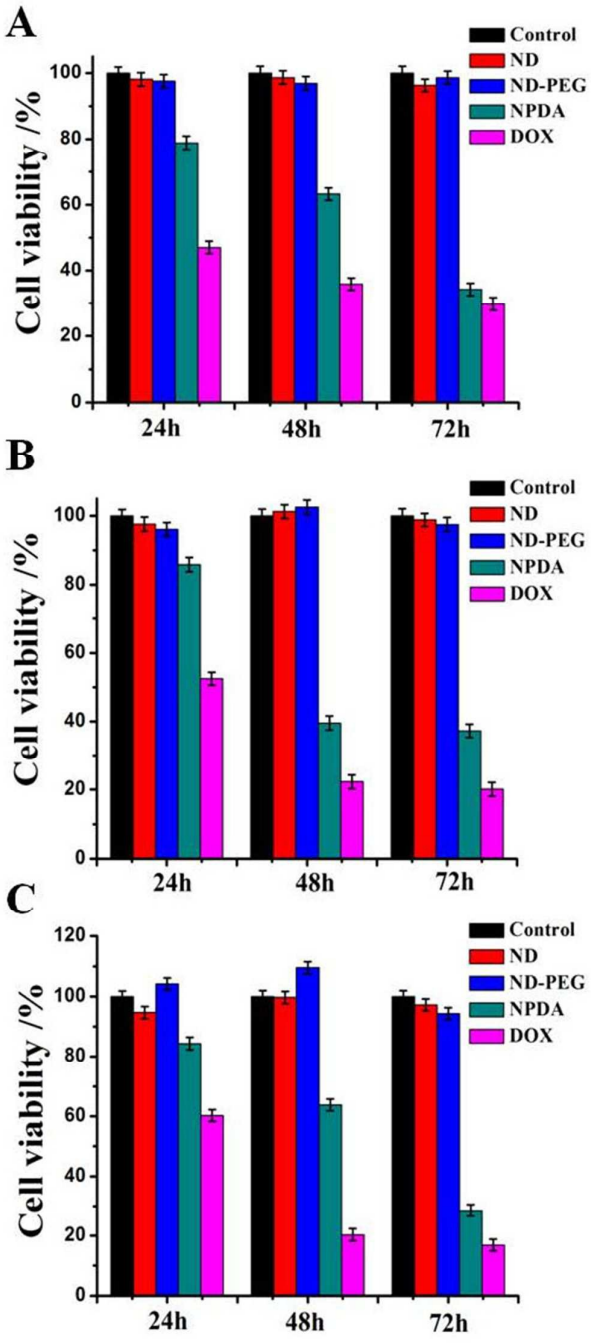

Fig. 5 Effect of free DOX and NPDA on HepG2, HeLa and MCF-7 cell viability for different time was measured by MTT assay. (A) HepG2, (B) HeLa and (C) MCF-7. Experiments were repeated three times and data are presented as the mean ± SD (for each group, n = 6).

relative cell viability declined monotonously with ascending the concentration of DOX.

Furthermore, morphologic observation results also demonstrate the effect of NPDA to cancer cells. Fig. S5 shows that cells treated with ND-PEG have intact cell membrane as well as control cells, which indicates that ND-PEG shows nontoxicity to cancer cells. On the contrary, the cells undergoing NPDA and free DOX have damaged and crushed cell membrane, which indicate that NPDA and free DOX can induce cell apoptosis as MTT assay verified.

In Vitro wound scratch assay

To determine the effect of cell migration by NPDA, the scratch assay was performed in the presence of NPDA (5 μg·mL^{-1} of DOX equivalent). As shown in Fig. 6A, the scratch width is evidently narrowed while MCF-7 cells treated by ND-PEG even if time increases, which is similar to the control group. However the scratch width is nearly essentially unchanged while MCF-7 cells were treated with NPDA and DOX, the migration inhibiting rate of NPDA and DOX were up to 76.05 % and 82.32 % as shown in Fig. 6B, respectively. Therefore, the NPDA can inhibit cell migration effectively.

Intracellular accumulation

Although the NPDA nanoparticles were found to be active, whether they have entered the cells or remained in the extracellular fluid was still unknown. Moreover, the therapeutic effect of DOX was dependent on its ability to inhibit the synthesis of nucleic acid through intercalation after entrance into nucleus. Therefore, to study whether the nanoparticles can enter living cells and DOX dissociated from NPDA nanoparticles, we used laser scanning confocal microscopy to record and examine the images of thedistribution of nanoparticles in the cells. In the experiment, using MCF-7 cells as a model, the cells were treated by NPDA with 5 μg·mL^{-1} of DOX equivalent for 2 h, 5 h and 21 h, respectively, or treated with free DOX (5 μg·mL^{-1}) for 1 h. Then cells were subjected to nuclear staining, followed by laser scanning confocal microscopy with excitation wavelength of 488 nm and emission wavelength at 530-580 nm. As shown in Fig. 7A, free DOX efficiently entered into the cells and located in the cell nucleus after treatment for 1 h which due to that small molecule could rapidly diffusion into the cell. In Fig. 7B, the green fluorescence signal of DOX from NPDA was distinctly observed in the cytoplasm alone after treatment with NPDA for 2 h and 5 h, but green fluorescence signal enhancement was seen at 5 h. When the incubation time was extended to 21 h, the green fluorescence was found both in the cytoplasm and nucleus and were mainly exhibited much accumulation in the nucleus. Such a result implied that NPDA moved inside the cells and were capable of ferrying the drug inside living cells efficiently. Then DOX molecules were detached from the NPDA and followed migrating into the nucleus. This would lead to a sustained functional drug release compared to free DOX, which is consistent with the gradual DOX release from NPDA complexes in PBS at 37 ℃ (Fig. 4). The result was also accordant with the previous report by us,[33, 38, 40, 44, 45] which indicated the potential applications of NPDA for controlled drug delivery.

Besides, in order to confirm the intracellular localization of NPDA, lysosomes were marked with Lyo-Tracker emitting in the red spectral region (655–755 nm) (shown in Fig. 7C, the middle imagine), The green fluorescent detection was for NPDA imaging, after chasing of their endocytosis for 5 h, some orange fluorescence in the cytoplasm observed from the Fig. 7C (The right imagine)

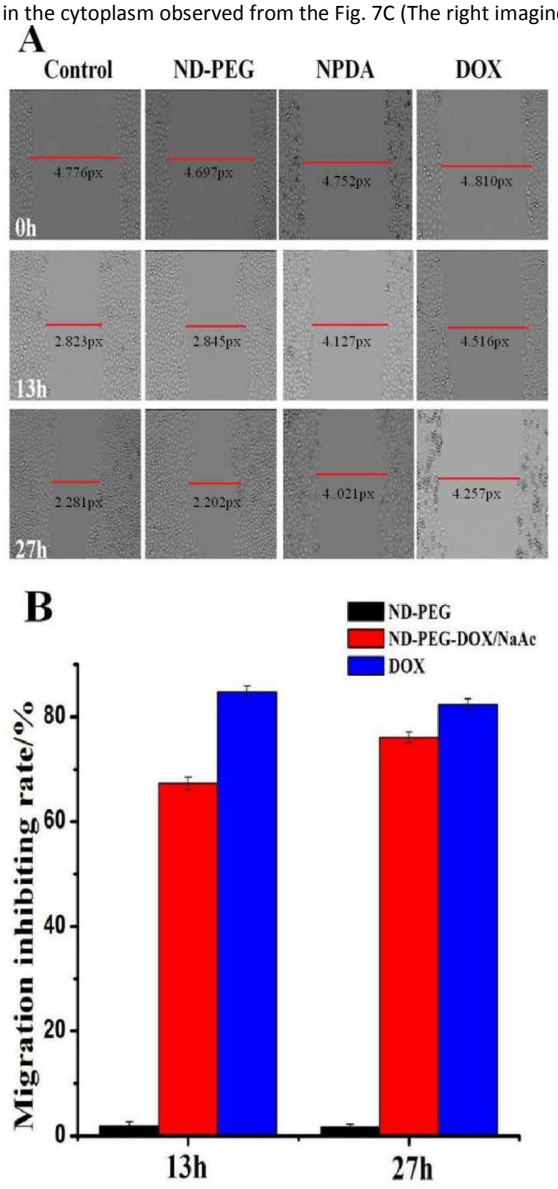

Fig. 6 The scratch assay of NPDA and free DOX with time. (A) Representative images of MCF-7 cells treatment by NPDA and free DOX, MCF-7 cells untreated as controls. (B) The migration inhibiting rate, where data were adopted from Fig. 6A.

showed the high colocalization of NPDA nanoparticles with lysosomes marked in red, which supports the fact that NPDA followed the course of the endocytosis cycle, and the finding hint that DOX was released from NPDA in the lysosomes with a low pH, escaped significantly from the lysosome membrane and entered the cytoplasm, finally DOX enters the nucleus, which is consistent with the DOX release behaviour in pH 4.5.

In addition, of importance, we found that NPDA could be internalized into cancer cells rather than normal cells, thereby achieving a selective drug accumulation into cancer cells to enhance tumor therapy efficiency and avoid damage to surrounding healthy cells and systemic toxicity, which was showed in Fig. 7D. From Fig. 7D one could see that NPDA nanoparticles barely internalized within cells by CHO cells compared with that of MCF-7 cells (Fig. 7B), suggesting that NPDA has the ability to selectively kill tumor cells and to alleviate the toxicity adverse effect of free DOX.

Due to the fact that side scatter (SS) by flow cytometry analysis can indicate the particle complexities within the cells, the cellular uptake of NPDA can be indirectly demonstrated by SS. Fig. 7E showed that the SS of NPDA uptake by MCF-7 cells after 1 h and 7 h incubation, respectively. After coculture with NPDA for 1 h, the value of SS only slightly increased, but it greatly increased after incubation 7 h. The result suggests that the NPDA nanoparticles indeed enter the cells and the cell uptake is a time-dependent process.

To further examine the uptake kinetics of NPDA in cancer cells, MCF-7 cells were treated with the same concentrations of NPDA for different time and analyzed by flow cytometer. As shown in Fig. S6, the cellular uptake of NPDA and free DOX were greatly strengthened with time increased and the fluorescence intensity reached a plateau at about 7 h for NPDA and 3 h for free DOX. Curve fitting by single exponent function showed that the rate constants (k) of the endocytosis for NPDA was about 0.34 h^{-1}, namely, the value of uptake half-life was near 2.06 h, while the value of uptake half-life of free DOX was about 0.93 h, which indicated that the uptake rate of NPDA was more than two times slower than free DOX. These results are related to cellular uptake pathways. The uptake of DOX occurs through an energy-independent passive diffusion mechanism,[45] while the NPDA nanoparticles can efficiently delivery the drug inside living cells via clathrin-dependent endocytosis pathway (Fig. S7).

Cell apoptosis and cell cycle

The effect of ND-PEG, NPDA and DOX on cell apoptosis was further investigated. In the apoptosis quadrant diagram, each quadrant represents the living cells, early apoptosis cells, late apoptosis cells and debris cells in a counter clockwise direction from the left bottom. As observed from the morphology of NPDA to cancer cells, free DOX and NPDA could induce cell apoptosis, after treatment for 48 h (Fig. S5). The apoptotic cells were further quantified using prodium iodide (PI)/Annexin V staining by flow cytometric analysis (Fig. 8A). As shown in Fig. 8A (b), the cells treated with ND-PEG displayed similar to the cells untreated, it could not induce cell apoptosis, implying that ND-PEG was nontoxic. While about 28 % cell apoptosis was induced by NPDA (Fig. 8A(c)) and a little lower compared to that induced by free DOX (38 %) (Fig. 8A(d)). The results again confirmed that DOX could efficiently release from NPDA in cells and resulted in cell apoptosis, and that mainly induced late cells apoptosis.

DOX could insert into the minor grooves of nucleic acids to inhibit their synthesis, and finally change the cell cycle.[46] Fig. 8B showed that cells treated with ND-PEG exhibited similar cell cycle with control cells, while NPDA and free DOX both significantly changed the cell cycle, NPDA (Fig. 8B(c)) resulting in 22.3 % reduction in the percentage of G2/M phase, 37.8 % increase in the percentage of G0/G1 phase and free DOX (Fig. 8B (d)) resulting in 17.4 % reduction in the percentage of G2/M phase, 22.4 % increase in the percentage of S phase, respectively. From Fig. 8B (e), we can see that the cells treated with NPDA increased at the percentage of G0/G1 phase,

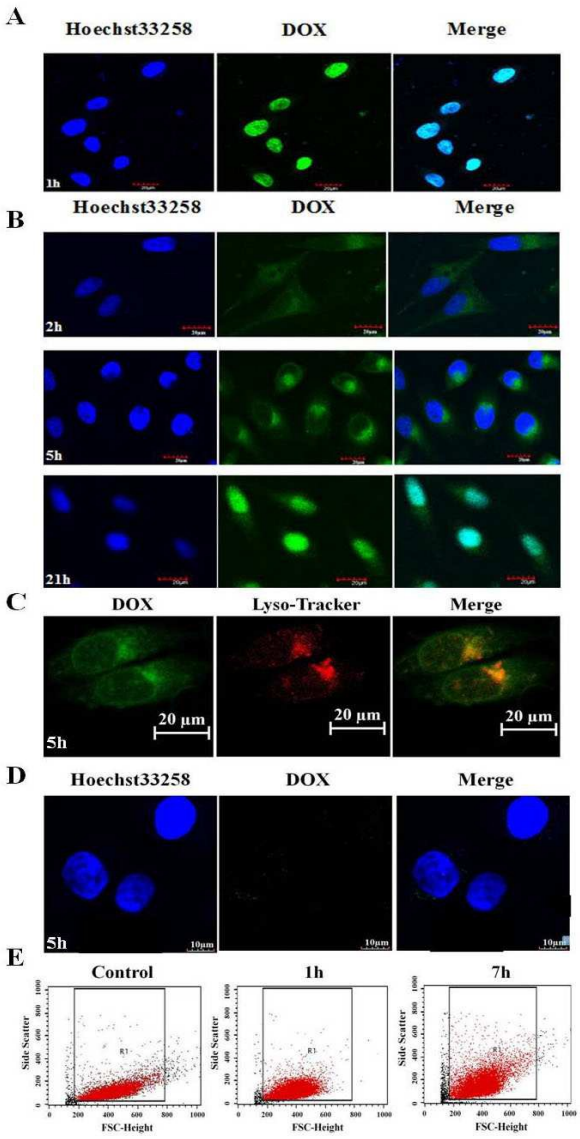

Fig. 7 Cellular uptake, distribution and uptake mechanism of NPDA nanoparticles. (A) Confocal laser scanning microscopy (CLSM) images of MCF-7 cells treated with free DOX for 1 h. (B) Confocal laser scanning microscopy (CLSM) images of MCF-7 cells treated with NPDA for 2 h, 5 h and 16 h, respectively. The images (A-B) in the left column show the cell nucleus dyed with Hoechst 33258; the middle column shows DOX fluorescence, and the right column shows the merge of the two previous images. (C) Intracellular accumulation of NPDA (3 $\mu g \cdot mL^{-1}$ of DOX equivalent) incubated with MCF-7 cells after endocytosis for 3 h. The images on the left column show DOX fluorescence from the NPDA nanoparticles; the middle column shows red lyso-tracker fluorescence; the right column shows the merge of the first two images. Scale bars: 20 μm. (D) Confocal laser scanning microscopy (CLSM) images of CHO cells treated with NPDA for 5 h.

The images in the left column show the cell nucleus dyed with Hoechst 33258; the middle column shows DOX fluorescence, and the right column shows the merge of the two previous images. (E) The variations of side scatter (SS) after MCF-7 cells were treated with NPDA for 1 h and 7 h was quantified from a minimum of 10000 cells by Cell Quest software using flow cytometry analysis, respectively. Y-axis is side scatter (SS), which indicated intracellular particle complexity; X-axis is forward scatter (FSC).

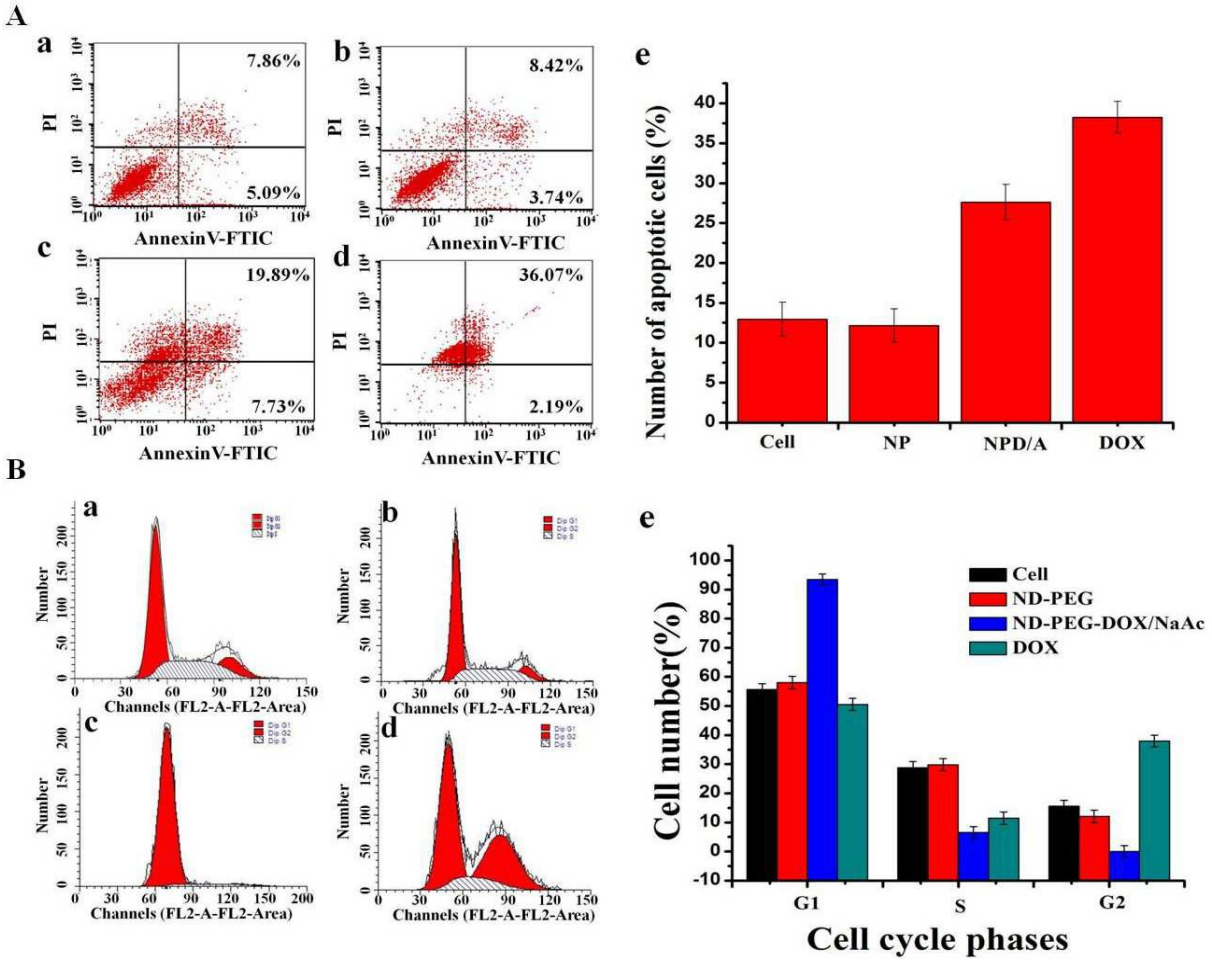

Fig. 8 Flow cytometry analysis. (A) Apoptosis of MCF-7 cells induced by ND-PEG (b), NPDA (c) and DOX (d) for 48 h, MCF-7 cells untreated as control (a), the number of apoptotic cells (e), where data were adopted from a,b,c and d. (B) Cell cycle of MCF-7 cells induced by ND-PEG (b), NPDA (c) and DOX (d), MCF-7 cells untreated as control (a), the cell cycle histogram (e), where data were adopted from a,b,c and d.

which implied that NPDA can change the cell cycle and mainly block in G0/G1 phase, while the group treated with free DOX was blocked in S phase. The results showed that both NPDA and free DOX emerged different cell cycle blocking and the difference belongs to different intracellular distributions for them.

Conclusions

In this work, a novel technique was presented for preparing ND-PEG-DOX/NaAc nanoparticle and achieving almost hundred percent in DOX drug loadings. Besides, the NPDA system exhibited excellent physiological stability and pH controlled drug release with high cytotoxicity to cancer cells. What is more, the results proved that NPDA preferentially accumulated in tumor cells but not normal cells. NPDA can enter living cells via clathrin-dependent endocytosis pathway and distribute in the lysosome and then sustained release DOX to nucleus to inhibit cell proliferation. This indicated that NPDA has a slow and sustained drug release capacity and selectively be internalized into cancer cells to improve the antitumor activity and reduce non-specific cytotoxicity to surrounding healthy tissues. It was also illustrated that NPDA can inhibit cell migration, induced cell apoptosis of mainly late apoptosis-dependence, and change the cell cycle compare to free drug. These studies will provide guidelines for developing smart nanocarriers for drug delivery applications.

Acknowledgements

This work is supported by the National Natural Science Foundation of China (Grant No. 21071091), Shanxi Science and Technology

Development Program (Grant No. 20130313021-1,201603D321025).

References

1 S. Punnen, J. E. Cowan, J. M. Chan, P. R. Carroll and M. R. Cooperberg, *Eur. Urol.,* 2015, **68**, 600-608.

2 R. S. Zheng, H. M. Zeng, S. W. Zhang, T. H. Chen and W. Q. Chen, *Cancer Lett.,* 2016, **370**, 33-38.

3 Q. L. Shi, T. G. Smith, J. D. Michonski, K. D. Stein, C. K. Kaw and C. S. Cleeland, *Cancer,* 2011, **117**, 2779-2790.

4 J. Ferlay, I. Soerjomataram, R. Dikshit, S. Eser, C. Mathers, M. Rebelo, D. M. Parkin, D. Forman and F. Bray, *Int. J. Cancer,* 2015, **136**, E359-E386.

5 H. L. Alaoui, O. U. I. Hassan, Y. W. Yang and P. Buchanan, *Biochim. Biophys. Acta.,* 2015, **1856**, 189-210.

6 D. J. Bharalia and S. A. Mousa, *Pharmacol. Ther.,* 2010, **128**, 324-335.

7 L. B. Peppas and J. O. Blanchette, *Adv. Drug Deliv. Rev.,* 2004, **56**, 1649-1659.

8 N. R. Jabir, S. Tabrez, G. M. d. Ashraf, S. Shakil, G. A. Damanhouri and M. A. Kama, *Int. J. Nanomed.,* 2012, **7**, 4391-4408.

9 R. Misra, S. Acharya and S. K. Sahoo, *Drug Discov. Today,* 2010, **15**, 842-850.

10 K. B. Sutradhar and M. L. Amin, *ISRN Nanotechnology,* 2014, **10**, 1-12.

11 R. Ranganathan, S. Madanmohan, A. Kesavan, G. Baskar, Y. R. Krishnamoorthy, R. Santosham, D. Ponraju, S. K. Rayala and G. Venkatraman, *Int. J. Nanomed.,* 2012, **7**, 1043-1060.

12 I. Brigger, C. Dubernet and P. Couvreur, *Adv. Drug Deliv. Rev.,* 2002, **54**, 631-651.

13 Y. Fukumori and H. Ichikawa, *Adv. Powder Technol.,* 2006, **17**, 1-28.

14 Z. Fan, P. P. Fu, H. T. Yua and P. C. Ray, *J. Food Drug Anal.,* 2014, **22**, 3-17.

15 N. Ahmed, H. Fessi and A. Elaissari, *Drug Discov. Today,* 2012, **17**, 928-934.

16 G. Zhao and B. L. Rodriguez, *Int. J. Nanomed.,* 2013, **8**, 61-71.

17 S. Kaur, C. Prasad, B. Balakrishnan and R. Banerjee, *Biomater. Sci.,* 2015, **3**, 955.

18 Y. Li, H. J. Wu, X. R. Yang, M. M. Jia, Y. X. Li, Y. Huang, J. Y. Lin, S. C. Wu and Z. Q. Hou, *Mol. Pharm.,* 2014, **11**, 2915-2927.

19 I. Mejac and C. D. Tran, *Anal. Chem.,* 2011, **83**, 3520-3527.

20 J. J. Wu, Y. R. Jian. Z. Sun and L. F. Feng, *ACS Appl. Mater. Interfaces,* 2013, **5**, 3519-3523.

21 S. F. Wang, Y. B. Li, J. J. Fan, Z. Y. Wang, X. Zeng, Y. Sun, P. Song and D. W. Ju, *Biomaterials,* 2014, **35**, 7588-7597.

22 A. A. Bhirde, V. Patel, J. Gavard, G. F. Zhang, A. A. Sousa, A. Masedunskas, R. D. Leapman, R. Weigert, J. S. Gutkind and J. F. Rusling, *ACS Nano,* 2009, **3**, 307-316.

23 T. M. Sun, Y. S. Zhang, B. Pang, D. C. Hyun, M. X. Yang and Y. N. Xia, *Angew. Chem. Int. Ed.,* 2014, **53**, 12320 -12364.

24 S. Abdalla, F. Al-Marzouki, A. A. Al-Ghamdi and A. Abdel-Daiem, *Nanoscale Res. Lett.,* 2015, **10**, 1-10.

25 X. C. Dong, W. Huang and P. Chen, *Nanoscale Res. Lett.,* 2011, **6**, 1-6.

26 O. D. Hendrickson, O. V. Morozova, A. V. Zherdev, A. I. Yaropolov, S. G. Klochkov, S. O. Bachurin and B. B. Dzantiev, *Fuller. Nanotub. Car. N.,* 2014, **23**, 658-668.

27 E. Pastor, E. Matveeva, A. Valle-Gallego, F. M. Goycoolea and M. Garcia-Fuentes, *Colloids Surf. B. Biointerfaces,* 2011, **88**, 601-609.

28 N. Mohan, C. S. Chen, H. H. Hsieh, Y. C. Wu and H. C. Chang, *Nano Lett.,* 2010, **10**, 3692.

29 T. Takimoto, T. Chano, S. Shimizu, H. Okabe, M. Ito, M. Morita, T. Kimura, T. Inubushi and N. Komatsu, *Chem. Mater.,* 2010, **22**, 3462-3471.

30 V. Vaijayanthimala, D. K. Lee, S. V. Kim, A. Yen, N. Tsai, D. Ho, H. C. Chang and O. Shenderova, *Expert Opin. Drug Deliv.,* 2015, **12**, 735-749.

31 H. B. Man, R. Lam, M. Chen, E. Osawa and D. Ho, *Phys. Status Solidi A.,* 2012, **9**, 1811-1818.

32 V. N. Mochalin, O. Shenderova, D. Ho and Y. Gogotsi, *Nat. Nanotechnol.,* 2012, **7**, 1-13.

33 Z. Q. Wang, Z. M. Tian, Y. Dong, L. Li, L. Tian, Y. Q. Li and B. S. Yang, *Diam. Relat. Mater.,* 2015, **58**, 84-93.

34 X. Y. Zhang, C. K. Fu, L. Feng, Y. Jia, L. Tao, Q. Huang, S. Li and Y. Wei, *Polymer,* 2012, **53**, 3178-3184.

35 G. Q. Qi, C. L. Liang, R. Y. Bao, Z. Y. Liu, W. Yang, B. H. Xie and M. B. Yang, *Sol. Energ. Mat. Sol. C.,* 2014, **123**, 171-177.

36 F. Mohandes and M. Salavati-Niasari, *J. Nanopart. Res.,* 2014, **16**, 1-12.

37 X. Y. Zhang, G. J. Zeng, J. W. Tian, Q. Wan, Q. Huang, K. Wang, Q. S. Zhang, M. Y. Liu, F. J. Deng and Y. Wei, *Appl Surf Sci.,* 2015, **351**, 425-432.

38 D. X. Wang, Y. L. Tong, Y. Q. Li, Z. M. Tian, R. X. Cao and B. S. Yang, *Diam. Relat. Mater.,* 2013, **36**, 26-34.

39 Z. Y. Xu, S. J. Zhu, M. W. Wang, Y. J. Li, P. Shi and X. Y. Huang, D. *ACS Appl. Mater. Interfaces,* 2015, **7**, 1355-1363.

40 Y. Dong, R. X. Cao, Y. Q. Li, Z. Q. Wang, L. Li and L. Tian, *RSC Adv.,* 2015, **5**, 82711-82716.

41 A. D. Salaam, P. T. J. Hwang, A. Poonawalla, H. N. Green, H. W. Jun and D. Dean, *Nanotechnology,* 2014, **25**, 1-12.

42 D. X. Wang, Y. Q. Li and B. S. Yang, *Acta Chim. Sinica.,* 2013, **71**, 782-786.

43 N. M. Dinana, F. Atyabi, M. R. Rouini, M. Amini, A. A. Golabchifar and R. Dinarvand, *Mater. Sci. Eng., C.,* 2014, **39**, 47-55.

44 Y. Q. Li, Y. L. Tong, R. X. Cao, Z. M. Tian, B. S. Yang and P. Yang, *Int. J. Nanomed.,* 2014, **9**, 1065-1082.

45 Y. Q. Li, X. P. Zhou, D. X. Wang, B. S. Yang and P. Yang, *J. Mater. Chem.,* 2011, **21**, 16406-16412.

46 H. C. Reinhardt, P. Hasskamp, I. Schmedding, S. Morandell, M. A. T. M. van Vugt, X. Z. Wang, R. Linding, S. E. Ong, D. Weaver, S. A. Carr and M. B. Yaffe, *Mol. Cell,* 2010, **40**, 34-49.

Highlight

Acetate ion enhance load and stability of doxorubicin onto PEGylated nanodiamond for selectively tumor intracellular controlled release and therapy